# Study of planar ground shock in different soils and its propagation around a rigid block

Leo Laine
ANKER – ZEMER Engineering A/S
Representing
Swedish Rescue Services Agency (SRSA)

Stugvägen 4, S-438 94 Härryda, Sweden
leo.laine@telia.com

This article focuses on how a planar ground shock propagates around a rigid block, buried in different type of soils. How the wave diffraction is progressing differently around the corner of the block, and how the loading of the floor varies for different soil types. The planar ground shock from a 125 kg of TNT per meter charge with the distance of five meter was analysed with a finite element solver. 16 soil types were analysed and varied from dry sand to fully saturated clay. Simulations showed that the diffraction became larger around the corner of the block when the soil has lower shear strength. Maximum pressure and impulse along the floor increased about 132 and 7 times respectively when dry sand was compared with fully saturated clay.

## INTRODUCTION

The Swedish Rescue Services Agency (SRSA) is responsible for the building regulations of the Swedish civil defence shelters. The shelters have specific regulations for how they are planned, built, equipped and maintained [1]. One of many regulations state what loading level the shelters should withstand: “The effect of a pressure wave corresponding to that produced by a 250 kg GP-bomb with 50 weight per cent TNT which burst freely outside at a distance of 5.0 meters from the outside of the shelter during free pressure release”. However, many of the shelters are designed as basements below ground surface. This is the reason why more knowledge about how the shock wave affects buried shelters is needed.

In the literature many studies can be found on how ground shock affects buried structures where the focus has usually been on the reflected pressure and its impulse on the vertical wall. Here in this article the focus has been on how a planar ground shock propagates around a rigid block buried in different soils, especially how the wave diffraction is occurring around the corner of the block, and how the loading of the floor varies for different soil types. The soil properties were varied from dry sand to wet clay. A total of 16 different soil properties were analysed.

The outline of the paper is as follows: The section FINITE ELEMENT MODEL is discussing how the model is setup. Section SOIL PROPERTIES shows how the different soil properties were generated. SIMULATIONS section analyses are carried out and results are shown. Finally CONCLUSIONS conclude the findings.

## FINITE ELEMENT MODEL

The finite element model tries to capture how the soil properties affect the propagation of a planar shock wave around a buried structure which could be represented by a shelter. The planar ground shock was analysed with a two dimensional axis symmetric explicit finite element solver with multi-material Euler formulation found in AUTODYN$^{TM}$ [2]. The focus in this study is on what effect different soil properties have on the propagation of a shock wave around a structure. Hence, the structural response is of minor importance and the structure is here simplified as a rigid block. A planar shock wave was generated by detonating 125 kg of TNT per meter which generated the shock wave in the soil and propagated towards the rigid block. The charge was modelled with the Jones-Wilkins-Lee Equation Of State (EOS). The distance between the rigid block and the planar charge was set to 5 meters. The height of the rigid wall was set to 3 meters and the floor length to 5 meters, see Fig. 1.

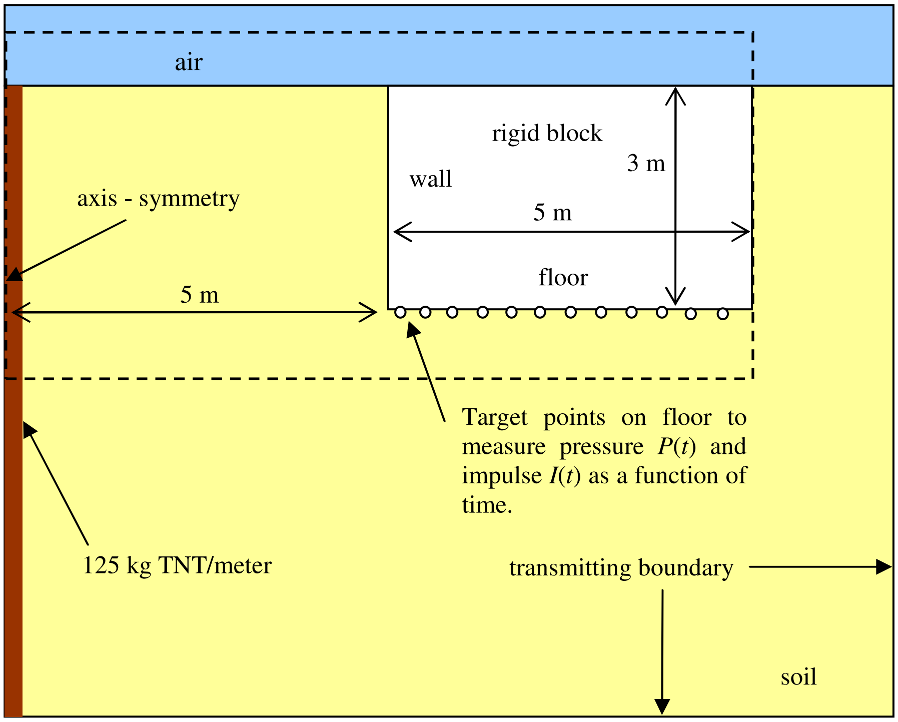

Fig. 1. Illustration of the principal layout of the finite element model.

The outer domain was 90 times 50 meters, distributed equally on soil and air, to allow the shock wave to propagate undisturbed for 100 ms. The air has an outflow boundary defined and the soil has a transmitting boundary. After sensitivity analysis of the element size 15 mm was chosen in the finer part of the domain which was 10 by 5 meters, illustrated in Fig. 1 with a dashed line. A total of 90 percent of the elements are found within the finer domain. The rigid block was modelled by unused elements. Target points were placed out along the outer wall and floor with a centre distance of 0.1 meter.

## SOIL PROPERTIES

In the study the soil properties were gradually changed from dry sand to fully saturated clay. A total of 16 different soil types were generated to study the effect on the shock wave and its diffraction around the rigid block when different soil properties are present. Two EOS were selected as a starting point when deriving the different soil properties. One was EOS for dry sand found in [3], here named E1 the second EOS was for fully saturated clay, here named E4. Linear scaling was used to derive two more EOS between these two extremes named E2 and E3. The gradual scaling of EOS is shown in Fig. 2. In total, four EOS were derived. Similarly the shear strength was linearly scaled between the dry sand [3] and the fully saturated clay to generate S1, S2, S3, and S4 respectively as illustrated in Fig. 3.

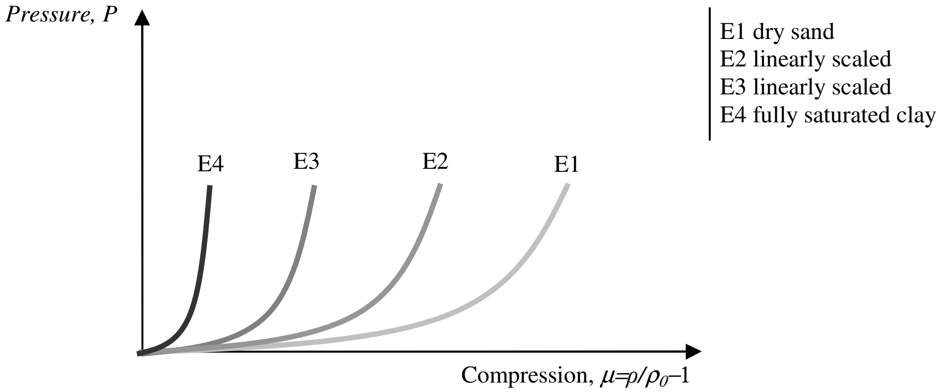

Fig. 2. Illustration of EOS and the linear scaling between the dry sand [3] and the fully saturated clay.

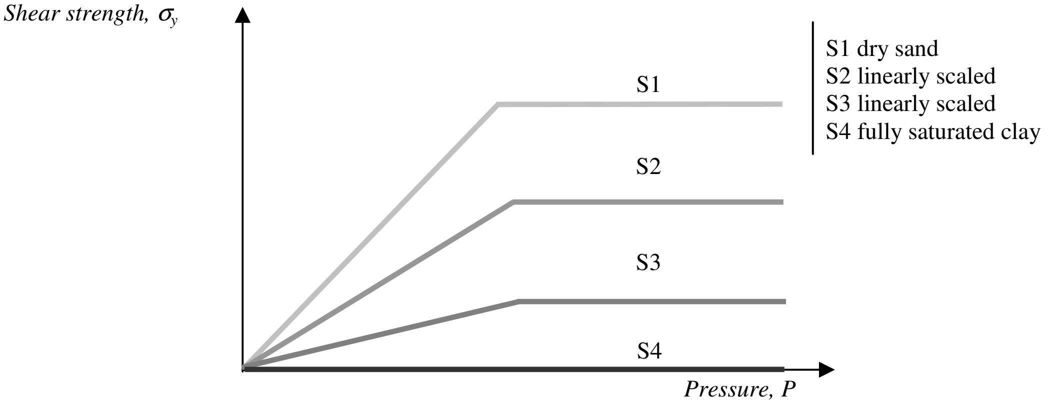

Fig. 3. Illustration of shear strength and the linear scaling between the dry sand [3] and the fully saturated clay.

The used material model was derived for modelling granular materials [4]. The material model allows the user to define the EOS as pressure as a function of density $P(\rho)$, shear strength as a function of pressure $\sigma_y(P)$, bulk sound speed as a function of density $c(\rho)$, and finally shear modulus as a function of density $G(\rho)$. Each one of the soil properties needed their specific $c(\rho)$ and $G(\rho)$. Additionally a hydro tensile limit of $P_{min}$= -1 kPa was defined for all soil properties due to the soils lack of handling any tensile pressure on a macro level. Table 1 gives all parameters used for each soil type. Only one of the soil properties i.e. dry sand or also called E1-S1 is fully derived by experiments [3] and [5]. These experiments were performed on sand found in Sjöbo Sweden. Tri-axial pressure cells up to about 100 MPa were used. The tests were performed first by isotropical loading and unloading to receive a fairly good picture of the porous EOS. The experiments were followed by tri-axial shear tests. Additionally the pressure and shear waves were measured during the tests by P- and S- transducers to get an idea how the bulk modulus and shear modulus varies with density and pressure. The fully saturated clay is only a generic soil property of what could be expected by fully saturated clay. However, the material properties in Table 1 will give a fairly good indication of what really influences the shock wave and its propagation around the rigid block.

| Soil type | E1-S1 | E1-S2 | E1-S3 | E1-S4 | E2-S1 | E2-S2 | E2-S3 | E2-S4 | E3-S1 | E3-S2 | E3-S3 | E3-S4 | E4-S1 | E4-S2 | E4-S3 | E4-S4 |
|---|---|---|---|---|---|---|---|---|---|---|---|---|---|---|---|---|
| $\rho_{ref}$ $(g/cm^3)$ | 2.641 | 2.641 | 2.641 | 2.641 | 2.467 | 2.467 | 2.467 | 2.467 | 2.264 | 2.264 | 2.264 | 2.264 | 2.027 | 2.027 | 2.027 | 2.027 |
| $\rho_{P\,1}$ | 1.674 | 1.674 | 1.674 | 1.674 | 1.752 | 1.752 | 1.752 | 1.752 | 1.830 | 1.830 | 1.830 | 1.830 | 1.908 | 1.908 | 1.908 | 1.908 |
| $\rho_2$ | 1.740 | 1.740 | 1.740 | 1.740 | 1.787 | 1.787 | 1.787 | 1.787 | 1.867 | 1.867 | 1.867 | 1.867 | 1.911 | 1.911 | 1.911 | 1.911 |
| $\rho_3$ | 1.874 | 1.874 | 1.874 | 1.874 | 1.836 | 1.836 | 1.836 | 1.836 | 1.903 | 1.903 | 1.903 | 1.903 | 1.913 | 1.913 | 1.913 | 1.913 |
| $\rho_4$ | 1.997 | 1.997 | 1.997 | 1.997 | 1.885 | 1.885 | 1.885 | 1.885 | 1.940 | 1.940 | 1.940 | 1.940 | 1.918 | 1.918 | 1.918 | 1.918 |
| $\rho_5$ | 2.144 | 2.144 | 2.144 | 2.144 | 1.927 | 1.927 | 1.927 | 1.927 | 1.976 | 1.976 | 1.976 | 1.976 | 1.928 | 1.928 | 1.928 | 1.928 |
| $\rho_6$ | 2.250 | 2.250 | 2.250 | 2.250 | 2.067 | 2.067 | 2.067 | 2.067 | 2.068 | 2.068 | 2.068 | 2.068 | 1.948 | 1.948 | 1.948 | 1.948 |
| $\rho_7$ | 2.380 | 2.380 | 2.380 | 2.380 | 2.208 | 2.208 | 2.208 | 2.208 | 2.178 | 2.178 | 2.178 | 2.178 | 1.987 | 1.987 | 1.987 | 1.987 |
| $\rho_8$ | 2.485 | 2.485 | 2.485 | 2.485 | 2.348 | 2.348 | 2.348 | 2.348 | 2.269 | 2.269 | 2.269 | 2.269 | 2.060 | 2.060 | 2.060 | 2.060 |
| $\rho_9$ | 2.585 | 2.585 | 2.585 | 2.585 | 2.488 | 2.488 | 2.488 | 2.488 | 2.361 | 2.361 | 2.361 | 2.361 | 2.233 | 2.233 | 2.233 | 2.233 |
| $\rho_{10}$ | 2.671 | 2.671 | 2.671 | 2.671 | 2.584 | 2.584 | 2.584 | 2.584 | 2.429 | 2.429 | 2.429 | 2.429 | 0 | 0 | 0 | 0 |
| $P_1$ $(kPa)$ | 0 | 0 | 0 | 0 | 0 | 0 | 0 | 0 | 0 | 0 | 0 | 0 | 0 | 0 | 0 | 0 |
| $P_2$ | 4.58E+03 | 4.58E+03 | 4.58E+03 | 4.58E+03 | 7.80E+03 | 7.80E+03 | 7.80E+03 | 7.80E+03 | 2.50E+04 | 2.50E+04 | 2.50E+04 | 2.50E+04 | 5.73E+03 | 5.73E+03 | 5.73E+03 | 5.73E+03 |
| $P_3$ | 1.50E+04 | 1.50E+04 | 1.50E+04 | 1.50E+04 | 2.20E+04 | 2.20E+04 | 2.20E+04 | 2.20E+04 | 5.80E+04 | 5.80E+04 | 5.80E+04 | 5.80E+04 | 1.15E+04 | 1.15E+04 | 1.15E+04 | 1.15E+04 |
| $P_4$ | 2.92E+04 | 2.92E+04 | 2.92E+04 | 2.92E+04 | 4.10E+04 | 4.10E+04 | 4.10E+04 | 4.10E+04 | 9.85E+04 | 9.85E+04 | 9.85E+04 | 9.85E+04 | 2.31E+04 | 2.31E+04 | 2.31E+04 | 2.31E+04 |
| $P_5$ | 5.92E+04 | 5.92E+04 | 5.92E+04 | 5.92E+04 | 6.25E+04 | 6.25E+04 | 6.25E+04 | 6.25E+04 | 1.40E+05 | 1.40E+05 | 1.40E+05 | 1.40E+05 | 4.66E+04 | 4.66E+04 | 4.66E+04 | 4.66E+04 |
| $P_6$ | 9.81E+04 | 9.81E+04 | 9.81E+04 | 9.81E+04 | 1.40E+05 | 1.40E+05 | 1.40E+05 | 1.40E+05 | 2.70E+05 | 2.70E+05 | 2.70E+05 | 2.70E+05 | 9.51E+04 | 9.51E+04 | 9.51E+04 | 9.51E+04 |
| $P_7$ | 1.79E+05 | 1.79E+05 | 1.79E+05 | 1.79E+05 | 2.62E+05 | 2.62E+05 | 2.62E+05 | 2.62E+05 | 4.35E+05 | 4.35E+05 | 4.35E+05 | 4.35E+05 | 1.98E+05 | 1.98E+05 | 1.98E+05 | 1.98E+05 |
| $P_8$ | 2.89E+05 | 2.89E+05 | 2.89E+05 | 2.89E+05 | 4.20E+05 | 4.20E+05 | 4.20E+05 | 4.20E+05 | 6.15E+05 | 6.15E+05 | 6.15E+05 | 6.15E+05 | 4.24E+05 | 4.24E+05 | 4.24E+05 | 4.24E+05 |
| $P_9$ | 4.50E+05 | 4.50E+05 | 4.50E+05 | 4.50E+05 | 6.50E+05 | 6.50E+05 | 6.50E+05 | 6.50E+05 | 8.38E+05 | 8.38E+05 | 8.38E+05 | 8.38E+05 | 1.18E+06 | 1.18E+06 | 1.18E+06 | 1.18E+06 |
| $P_{10}$ | 6.51E+05 | 6.51E+05 | 6.51E+05 | 6.51E+05 | 8.90E+05 | 8.90E+05 | 8.90E+05 | 8.90E+05 | 1.09E+06 | 1.09E+06 | 1.09E+06 | 1.09E+06 | 0 | 0 | 0 | 0 |
| $\rho_{c1}$ $(g/cm^3)$ | 1.674 | 1.674 | 1.674 | 1.674 | 1.752 | 1.752 | 1.752 | 1.752 | 1.830 | 1.830 | 1.830 | 1.830 | 1.908 | 1.908 | 1.908 | 1.908 |
| $\rho_{c2}$ | 1.746 | 1.746 | 1.746 | 1.746 | 1.770 | 1.770 | 1.770 | 1.770 | 1.846 | 1.846 | 1.846 | 1.846 | 1.908 | 1.908 | 1.908 | 1.908 |
| $\rho_{c3}$ | 2.086 | 2.086 | 2.086 | 2.086 | 1.812 | 1.812 | 1.812 | 1.812 | 1.866 | 1.866 | 1.866 | 1.866 | 1.908 | 1.908 | 1.908 | 1.908 |
| $\rho_{c4}$ | 2.147 | 2.147 | 2.147 | 2.147 | 1.853 | 1.853 | 1.853 | 1.853 | 1.879 | 1.879 | 1.879 | 1.879 | 1.908 | 1.908 | 1.908 | 1.908 |
| $\rho_{c5}$ | 2.300 | 2.300 | 2.300 | 2.300 | 1.883 | 1.883 | 1.883 | 1.883 | 1.942 | 1.942 | 1.942 | 1.942 | 1.909 | 1.909 | 1.909 | 1.909 |
| $\rho_{c6}$ | 2.572 | 2.572 | 2.572 | 2.572 | 2.109 | 2.109 | 2.109 | 2.109 | 2.020 | 2.020 | 2.020 | 2.020 | 1.913 | 1.913 | 1.913 | 1.913 |
| $\rho_{c7}$ | 2.598 | 2.598 | 2.598 | 2.598 | 2.230 | 2.230 | 2.230 | 2.230 | 2.084 | 2.084 | 2.084 | 2.084 | 1.923 | 1.923 | 1.923 | 1.923 |
| $\rho_{c8}$ | 2.635 | 2.635 | 2.635 | 2.635 | 2.354 | 2.354 | 2.354 | 2.354 | 2.185 | 2.185 | 2.185 | 2.185 | 1.963 | 1.963 | 1.963 | 1.963 |
| $\rho_{c9}$ | 2.641 | 2.641 | 2.641 | 2.641 | 2.467 | 2.467 | 2.467 | 2.467 | 2.264 | 2.264 | 2.264 | 2.264 | 2.027 | 2.027 | 2.027 | 2.027 |
| $\rho_{c10}$ | 2.800 | 2.800 | 2.800 | 2.800 | 2.584 | 2.584 | 2.584 | 2.584 | 2.336 | 2.336 | 2.336 | 2.336 | 2.046 | 2.046 | 2.046 | 2.046 |
| $c_1$ $(m/s)$ | 265.2 | 265.2 | 265.2 | 265.2 | 472.8 | 472.8 | 472.8 | 472.8 | 827.4 | 827.4 | 827.4 | 827.4 | 1499.9 | 1499.9 | 1499.9 | 1499.9 |
| $c_2$ | 852.1 | 852.1 | 852.1 | 852.1 | 676.3 | 676.3 | 676.3 | 676.3 | 1107.8 | 1107.8 | 1107.8 | 1107.8 | 1505.8 | 1505.8 | 1505.8 | 1505.8 |
| $c_3$ | 1721.7 | 1721.7 | 1721.7 | 1721.7 | 960.8 | 960.8 | 960.8 | 960.8 | 1251.2 | 1251.2 | 1251.2 | 1251.2 | 1515.2 | 1515.2 | 1515.2 | 1515.2 |
| $c_4$ | 1875.5 | 1875.5 | 1875.5 | 1875.5 | 1126.7 | 1126.7 | 1126.7 | 1126.7 | 1274.5 | 1274.5 | 1274.5 | 1274.5 | 1533.2 | 1533.2 | 1533.2 | 1533.2 |
| $c_5$ | 2264.8 | 2264.8 | 2264.8 | 2264.8 | 1188.0 | 1188.0 | 1188.0 | 1188.0 | 1464.1 | 1464.1 | 1464.1 | 1464.1 | 1569.4 | 1569.4 | 1569.4 | 1569.4 |
| $c_6$ | 2956.1 | 2956.1 | 2956.1 | 2956.1 | 1632.0 | 1632.0 | 1632.0 | 1632.0 | 1658.6 | 1658.6 | 1658.6 | 1658.6 | 1636.4 | 1636.4 | 1636.4 | 1636.4 |
| $c_7$ | 3112.2 | 3112.2 | 3112.2 | 3112.2 | 1892.4 | 1892.4 | 1892.4 | 1892.4 | 1822.9 | 1822.9 | 1822.9 | 1822.9 | 1768.5 | 1768.5 | 1768.5 | 1768.5 |
| $c_8$ | 4600.0 | 4600.0 | 4600.0 | 4600.0 | 2201.7 | 2201.7 | 2201.7 | 2201.7 | 2182.5 | 2182.5 | 2182.5 | 2182.5 | 2095.2 | 2095.2 | 2095.2 | 2095.2 |
| $c_9$ | 4634.0 | 4634.0 | 4634.0 | 4634.0 | 2753.4 | 2753.4 | 2753.4 | 2753.4 | 2563.4 | 2563.4 | 2563.4 | 2563.4 | 2388.5 | 2388.5 | 2388.5 | 2388.5 |
| $c_{10}$ | 4634.0 | 4634.0 | 4634.0 | 4634.0 | 2753.4 | 2753.4 | 2753.4 | 2753.4 | 2563.4 | 2563.4 | 2563.4 | 2563.4 | 2388.5 | 2388.5 | 2388.5 | 2388.5 |
| $P\,\sigma_{y1}$ $(kPa)$ | 0 | 0 | 0 | 0 | 0 | 0 | 0 | 0 | 0 | 0 | 0 | 0 | 0 | 0 | 0 | 0 |
| $P\,\sigma_{y2}$ | 3.40E+03 | 3.40E+03 | 3.40E+03 | 3.40E+03 | 3.40E+03 | 3.40E+03 | 3.40E+03 | 3.40E+03 | 3.40E+03 | 3.40E+03 | 3.40E+03 | 3.40E+03 | 3.40E+03 | 3.40E+03 | 3.40E+03 | 3.40E+03 |
| $P\,\sigma_{y3}$ | 3.49E+04 | 3.49E+04 | 3.49E+04 | 3.49E+04 | 3.49E+04 | 3.49E+04 | 3.49E+04 | 3.49E+04 | 3.49E+04 | 3.49E+04 | 3.49E+04 | 3.49E+04 | 3.49E+04 | 3.49E+04 | 3.49E+04 | 3.49E+04 |
| $P\,\sigma_{y4}$ | 1.01E+05 | 1.01E+05 | 1.01E+05 | 1.01E+05 | 1.01E+05 | 1.01E+05 | 1.01E+05 | 1.01E+05 | 1.01E+05 | 1.01E+05 | 1.01E+05 | 1.01E+05 | 1.01E+05 | 1.01E+05 | 1.01E+05 | 1.01E+05 |
| $P\,\sigma_{y5}$ | 1.85E+05 | 1.85E+05 | 1.85E+05 | 1.85E+05 | 1.85E+05 | 1.85E+05 | 1.85E+05 | 1.85E+05 | 1.85E+05 | 1.85E+05 | 1.85E+05 | 1.85E+05 | 1.85E+05 | 1.85E+05 | 1.85E+05 | 1.85E+05 |
| $P\,\sigma_{y6}$ | 5.00E+05 | 5.00E+05 | 5.00E+05 | 5.00E+05 | 5.00E+05 | 5.00E+05 | 5.00E+05 | 5.00E+05 | 5.00E+05 | 5.00E+05 | 5.00E+05 | 5.00E+05 | 5.00E+05 | 5.00E+05 | 5.00E+05 | 5.00E+05 |
| $P\,\sigma_{y7}$ | 0 | 0 | 0 | 0 | 0 | 0 | 0 | 0 | 0 | 0 | 0 | 0 | 0 | 0 | 0 | 0 |
| $P\,\sigma_{y8}$ | 0 | 0 | 0 | 0 | 0 | 0 | 0 | 0 | 0 | 0 | 0 | 0 | 0 | 0 | 0 | 0 |
| $P\,\sigma_{y9}$ | 0 | 0 | 0 | 0 | 0 | 0 | 0 | 0 | 0 | 0 | 0 | 0 | 0 | 0 | 0 | 0 |
| $P\,\sigma_{y10}$ | 0 | 0 | 0 | 0 | 0 | 0 | 0 | 0 | 0 | 0 | 0 | 0 | 0 | 0 | 0 | 0 |
| $\sigma_{y1}$ $(kPa)$ | 0.00E+00 | 0.00E+00 | 0.00E+00 | 0.00E+00 | 0.00E+00 | 0.00E+00 | 0.00E+00 | 0.00E+00 | 0.00E+00 | 0.00E+00 | 0.00E+00 | 0.00E+00 | 0.00E+00 | 0.00E+00 | 0.00E+00 | 0.00E+00 |
| $\sigma_{y2}$ | 4.24E+03 | 2.82E+03 | 1.41E+03 | 4.24E+01 | 4.24E+03 | 2.82E+03 | 1.41E+03 | 4.24E+01 | 4.24E+03 | 2.82E+03 | 1.41E+03 | 4.24E+01 | 4.24E+03 | 2.82E+03 | 1.41E+03 | 4.24E+01 |
| $\sigma_{y3}$ | 4.47E+04 | 2.98E+04 | 1.49E+04 | 4.47E+02 | 4.47E+04 | 2.98E+04 | 1.49E+04 | 4.47E+02 | 4.47E+04 | 2.98E+04 | 1.49E+04 | 4.47E+02 | 4.47E+04 | 2.98E+04 | 1.49E+04 | 4.47E+02 |
| $\sigma_{y4}$ | 1.24E+05 | 8.27E+04 | 4.13E+04 | 1.24E+03 | 1.24E+05 | 8.27E+04 | 4.13E+04 | 1.24E+03 | 1.24E+05 | 8.27E+04 | 4.13E+04 | 1.24E+03 | 1.24E+05 | 8.27E+04 | 4.13E+04 | 1.24E+03 |
| $\sigma_{y5}$ | 2.26E+05 | 1.51E+05 | 7.53E+04 | 2.26E+03 | 2.26E+05 | 1.51E+05 | 7.53E+04 | 2.26E+03 | 2.26E+05 | 1.51E+05 | 7.53E+04 | 2.26E+03 | 2.26E+05 | 1.51E+05 | 7.53E+04 | 2.26E+03 |
| $\sigma_{y6}$ | 2.26E+05 | 1.51E+05 | 7.53E+04 | 2.26E+03 | 2.26E+05 | 1.51E+05 | 7.53E+04 | 2.26E+03 | 2.26E+05 | 1.51E+05 | 7.53E+04 | 2.26E+03 | 2.26E+05 | 1.51E+05 | 7.53E+04 | 2.26E+03 |
| $\sigma_{y7}$ | 0 | 0 | 0 | 0 | 0 | 0 | 0 | 0 | 0 | 0 | 0 | 0 | 0 | 0 | 0 | 0 |
| $\sigma_{y8}$ | 0 | 0 | 0 | 0 | 0 | 0 | 0 | 0 | 0 | 0 | 0 | 0 | 0 | 0 | 0 | 0 |
| $\sigma_{y9}$ | 0 | 0 | 0 | 0 | 0 | 0 | 0 | 0 | 0 | 0 | 0 | 0 | 0 | 0 | 0 | 0 |
| $\sigma_{y10}$ | 0 | 0 | 0 | 0 | 0 | 0 | 0 | 0 | 0 | 0 | 0 | 0 | 0 | 0 | 0 | 0 |
| $\rho_{G1}$ $(g/cm^3)$ | 1.674 | 1.674 | 1.674 | 1.674 | 1.752 | 1.752 | 1.752 | 1.752 | 1.830 | 1.830 | 1.830 | 1.830 | 1.908 | 1.908 | 1.908 | 1.908 |
| $\rho_{G2}$ | 1.746 | 1.746 | 1.746 | 1.746 | 1.770 | 1.770 | 1.770 | 1.770 | 1.846 | 1.846 | 1.846 | 1.846 | 1.908 | 1.908 | 1.908 | 1.908 |
| $\rho_{G3}$ | 2.086 | 2.086 | 2.086 | 2.086 | 1.812 | 1.812 | 1.812 | 1.812 | 1.866 | 1.866 | 1.866 | 1.866 | 1.908 | 1.908 | 1.908 | 1.908 |
| $\rho_{G4}$ | 2.147 | 2.147 | 2.147 | 2.147 | 1.853 | 1.853 | 1.853 | 1.853 | 1.879 | 1.879 | 1.879 | 1.879 | 1.908 | 1.908 | 1.908 | 1.908 |
| $\rho_{G5}$ | 2.300 | 2.300 | 2.300 | 2.300 | 1.883 | 1.883 | 1.883 | 1.883 | 1.942 | 1.942 | 1.942 | 1.942 | 1.909 | 1.909 | 1.909 | 1.909 |
| $\rho_{G6}$ | 2.572 | 2.572 | 2.572 | 2.572 | 2.109 | 2.109 | 2.109 | 2.109 | 2.020 | 2.020 | 2.020 | 2.020 | 1.913 | 1.913 | 1.913 | 1.913 |
| $\rho_{G7}$ | 2.598 | 2.598 | 2.598 | 2.598 | 2.230 | 2.230 | 2.230 | 2.230 | 2.084 | 2.084 | 2.084 | 2.084 | 1.923 | 1.923 | 1.923 | 1.923 |
| $\rho_{G8}$ | 2.635 | 2.635 | 2.635 | 2.635 | 2.354 | 2.354 | 2.354 | 2.354 | 2.185 | 2.185 | 2.185 | 2.185 | 1.963 | 1.963 | 1.963 | 1.963 |
| $\rho_{G9}$ | 2.641 | 2.641 | 2.641 | 2.641 | 2.467 | 2.467 | 2.467 | 2.467 | 2.264 | 2.264 | 2.264 | 2.264 | 2.027 | 2.027 | 2.027 | 2.027 |
| $\rho_{G10}$ | 2.800 | 2.800 | 2.800 | 2.800 | 2.584 | 2.584 | 2.584 | 2.584 | 2.336 | 2.336 | 2.336 | 2.336 | 2.046 | 2.046 | 2.046 | 2.046 |
| $G_1$ $(kPa)$ | 7.69E+04 | 5.13E+04 | 2.56E+04 | 7.69E+02 | 7.69E+04 | 5.13E+04 | 2.56E+04 | 7.69E+02 | 7.69E+04 | 5.13E+04 | 2.56E+04 | 7.69E+02 | 7.69E+04 | 5.13E+04 | 2.56E+04 | 7.69E+02 |
| $G_2$ | 8.69E+05 | 5.80E+05 | 2.90E+05 | 8.69E+03 | 3.46E+05 | 2.31E+05 | 1.15E+05 | 3.46E+03 | 4.76E+05 | 3.18E+05 | 1.59E+05 | 4.76E+03 | 7.87E+04 | 5.25E+04 | 2.62E+04 | 7.87E+02 |
| $G_3$ | 4.03E+06 | 2.69E+06 | 1.34E+06 | 4.03E+04 | 9.61E+05 | 6.40E+05 | 3.20E+05 | 9.61E+03 | 9.51E+05 | 6.34E+05 | 3.17E+05 | 9.51E+03 | 8.46E+04 | 5.64E+04 | 2.82E+04 | 8.46E+02 |
| $G_4$ | 4.91E+06 | 3.27E+06 | 1.64E+06 | 4.91E+04 | 1.47E+06 | 9.80E+05 | 4.90E+05 | 1.47E+04 | 1.22E+06 | 8.13E+05 | 4.07E+05 | 1.22E+04 | 1.07E+05 | 7.11E+04 | 3.56E+04 | 1.07E+03 |
| $G_5$ | 7.77E+06 | 5.18E+06 | 2.59E+06 | 7.77E+04 | 1.85E+06 | 1.23E+06 | 6.16E+05 | 1.85E+04 | 2.52E+06 | 1.68E+06 | 8.39E+05 | 2.52E+04 | 1.92E+05 | 1.28E+05 | 6.40E+04 | 1.92E+03 |
| $G_6$ | 1.48E+07 | 9.87E+06 | 4.93E+06 | 1.48E+05 | 5.10E+06 | 3.40E+06 | 1.70E+06 | 5.10E+04 | 4.17E+06 | 2.78E+06 | 1.39E+06 | 4.17E+04 | 4.85E+05 | 3.24E+05 | 1.62E+05 | 4.85E+03 |
| $G_7$ | 1.66E+07 | 1.10E+07 | 5.52E+06 | 1.66E+05 | 8.32E+06 | 5.54E+06 | 2.77E+06 | 8.32E+04 | 6.65E+06 | 4.43E+06 | 2.22E+06 | 6.65E+04 | 1.38E+06 | 9.17E+05 | 4.59E+05 | 1.38E+04 |
| $G_8$ | 3.67E+07 | 2.45E+07 | 1.22E+07 | 3.67E+05 | 1.26E+07 | 8.42E+06 | 4.21E+06 | 1.26E+05 | 1.20E+07 | 8.01E+06 | 4.01E+06 | 1.20E+05 | 4.57E+06 | 3.05E+06 | 1.52E+06 | 4.57E+04 |
| $G_9$ | 3.73E+07 | 2.49E+07 | 1.24E+07 | 3.73E+05 | 3.73E+07 | 2.49E+07 | 1.24E+07 | 3.73E+05 | 3.73E+07 | 2.49E+07 | 1.24E+07 | 3.73E+05 | 3.73E+07 | 2.49E+07 | 1.24E+07 | 3.73E+05 |
| $G_{10}$ | 3.73E+07 | 2.49E+07 | 1.24E+07 | 3.73E+05 | 3.73E+07 | 2.49E+07 | 1.24E+07 | 3.73E+05 | 3.73E+07 | 2.49E+07 | 1.24E+07 | 3.73E+05 | 3.73E+07 | 2.49E+07 | 1.24E+07 | 3.73E+05 |
| $P_{minfail}$ $(kPa)$ | -1 | -1 | -1 | -1 | -1 | -1 | -1 | -1 | -1 | -1 | -1 | -1 | -1 | -1 | -1 | -1 |

Table 1. The 16 derived and used soil properties.

## SIMULATIONS

A total of 16 simulations were performed with same set up as explained in the Section FINITE ELEMENT MODEL except for the used soil type. The focus with the simulations was to get an idea what influence the soil properties have on the maximum pressure and maximum impulse along the floor and also how the diffraction around the corner of the rigid block is affected of the soil properties.

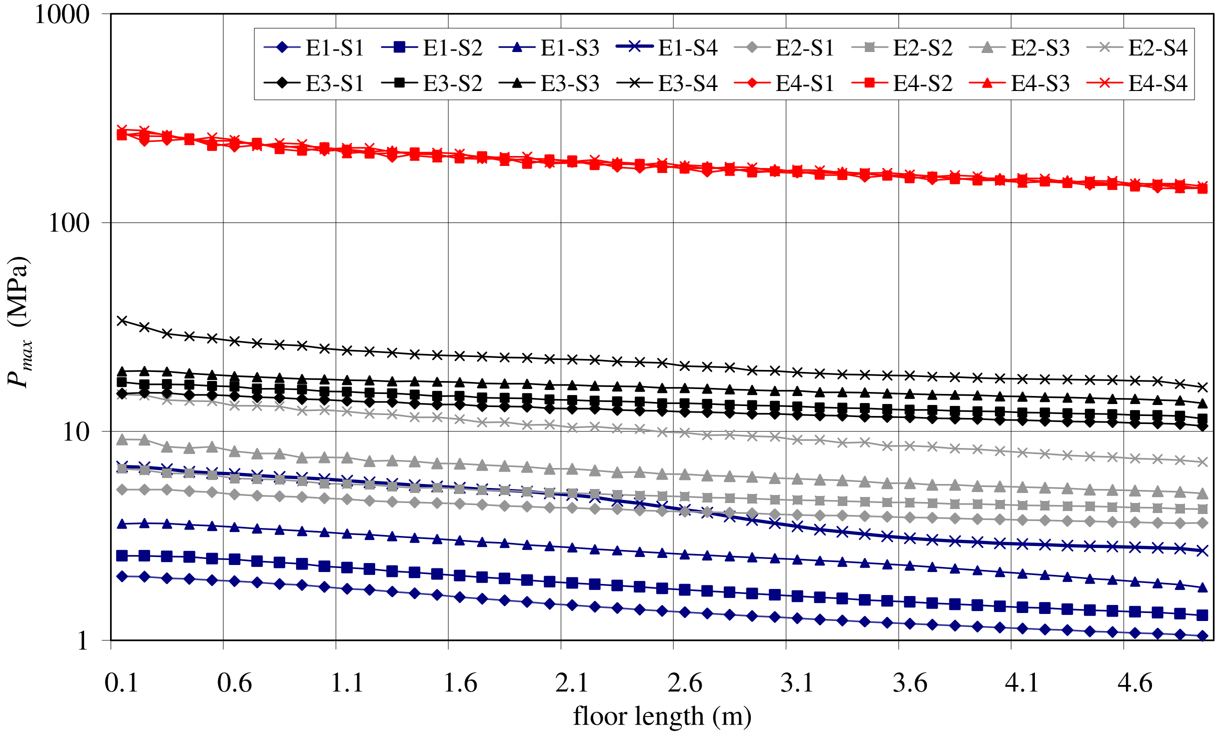

Fig. 4. Maximum pressure along the floor for all 16 different soil types. The pressure is given in logarithmic scale.

The change in maximum floor pressure and maximum impulse was studied for all 16 soil types and the results showed that the floor pressure increased most with ‘stiffer’ EOS, i.e. the soil types which needed less compression to reach same pressure. Fig. 4 shows how maximum pressure varies along the floor for different soil types. The maximum pressure increased in average 132 times when results using E1-S1 (EOS from dry sand combined with strength model from dry sand) and E4-S1 (EOS from fully saturated clay combined with strength model from dry sand) are compared.

The shear strength also influences the level of the maximum pressure of the floor. Fig. 5 shows how the maximum pressure varies for all soil types with E1, EOS for dry sand but the shear strength varied from dry sand to fully saturated clay. One can observe a significant increase in pressure, in average about three times higher for E1-S4 than for E1-S1. When the EOS is becoming stiffer the effect is reduced, and when the EOS is equal to fully saturated clay it is erased, see Fig. 6.

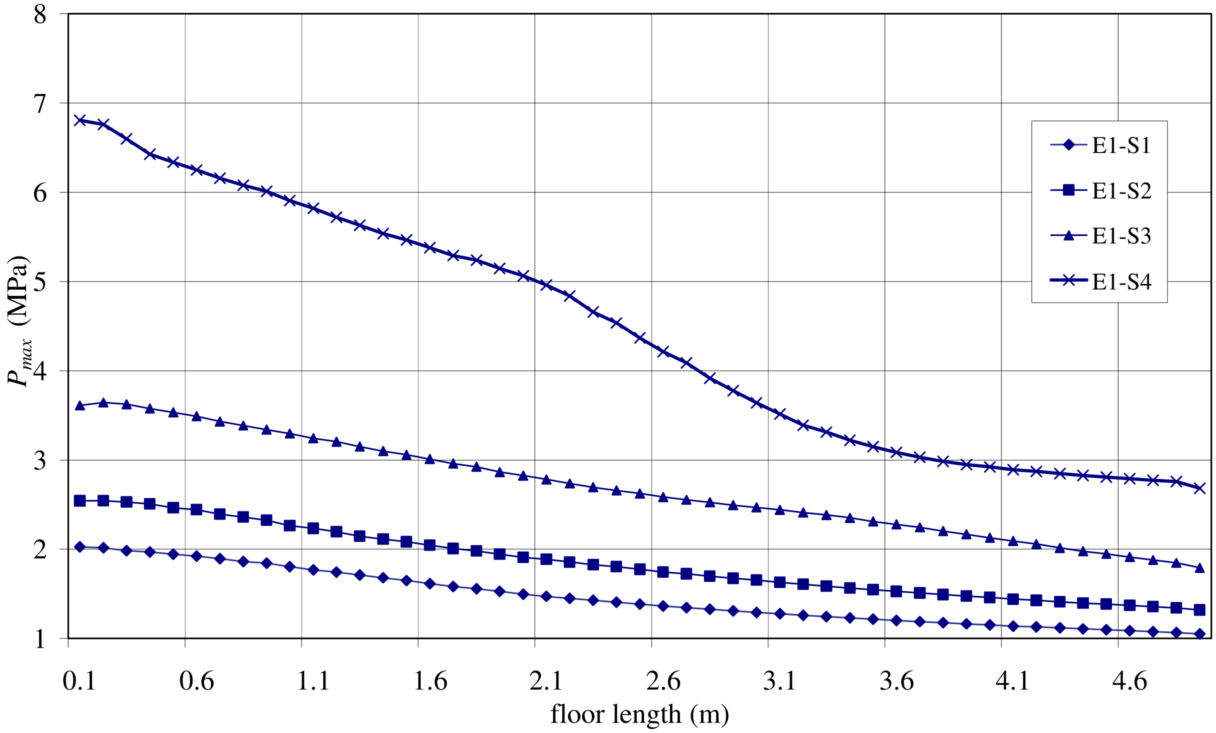

Fig. 5. Maximum pressure along the floor for EOS dry sand and the shear strength varied, E1-S*i*.

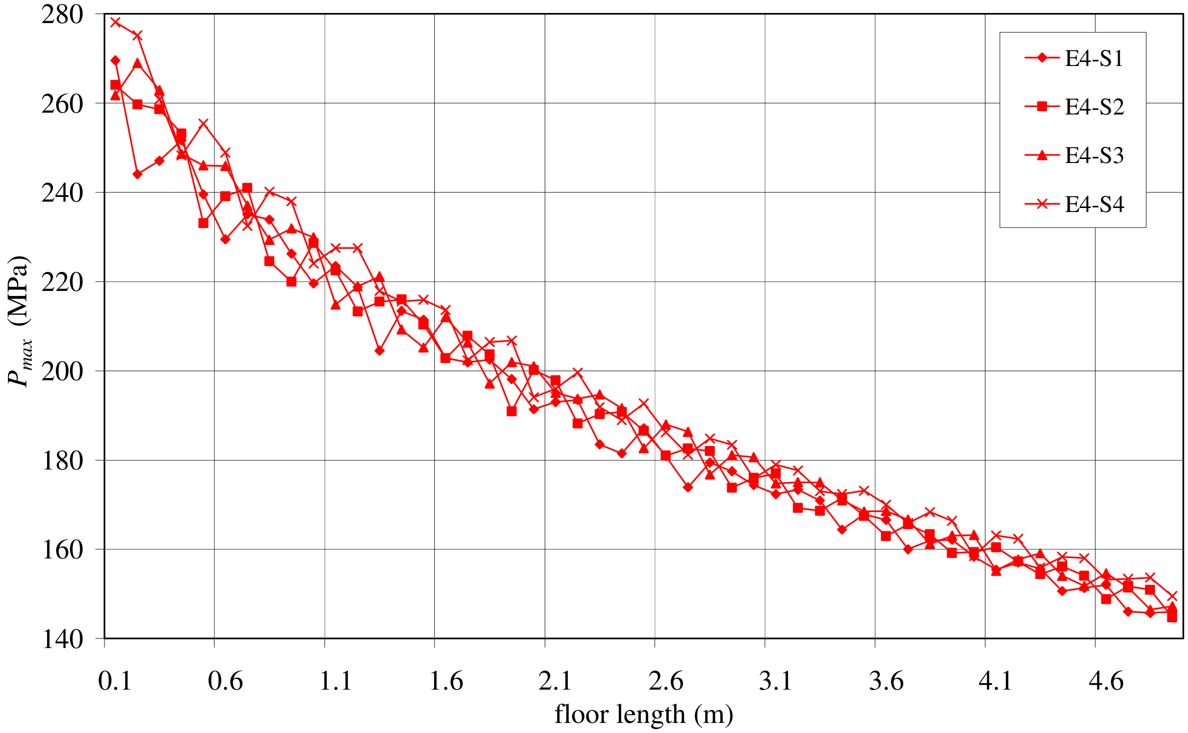

Fig. 6. Maximum pressure along the floor for EOS fully saturated clay and the shear strength varied, E4-S*i*.

The maximum impulse increases similarly as maximum pressure with stiffer EOS, see Fig. 7. The maximum impulse increase in average about seven times when E1-S1 is compared with E4-S1. The shear strength also influences the maximum impulse. When the EOS is kept constant with dry sand and the shear strength is varied the maximum impulse increase in average three times when E1-S1 is compared with E1-S4, see Fig. 8.

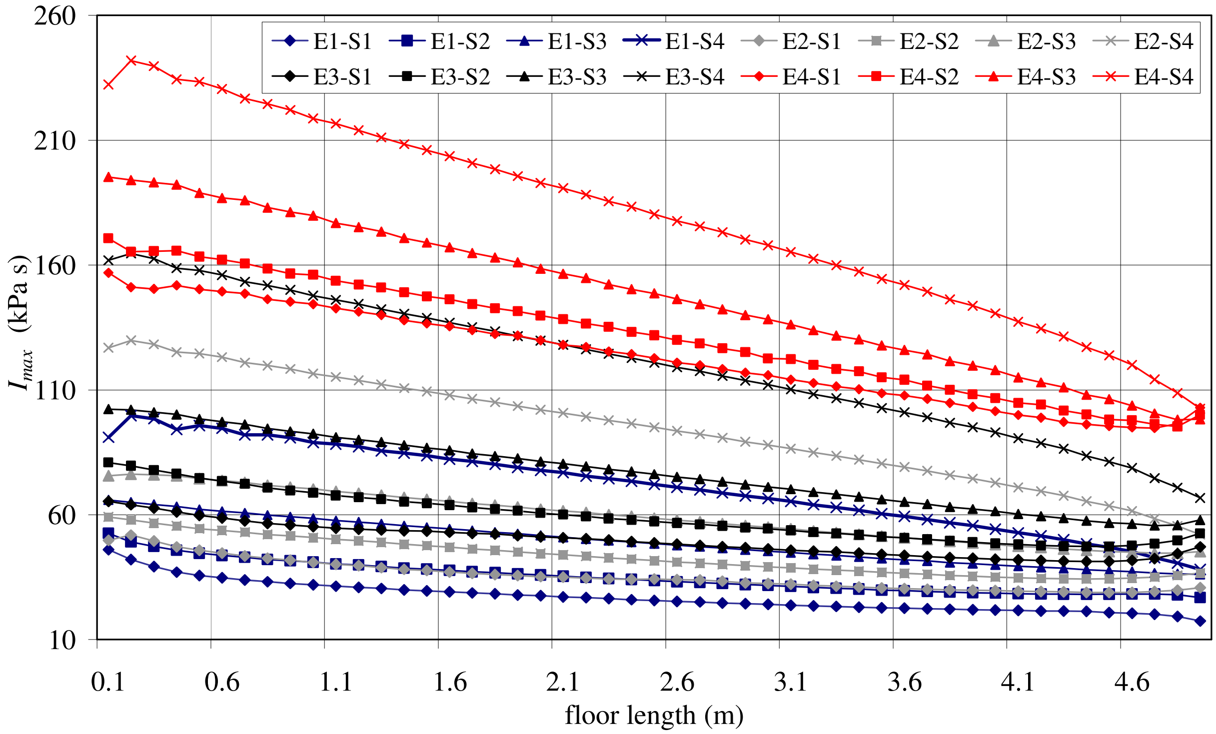

Fig. 7. Maximum impulse along the floor for all 16 different soil types

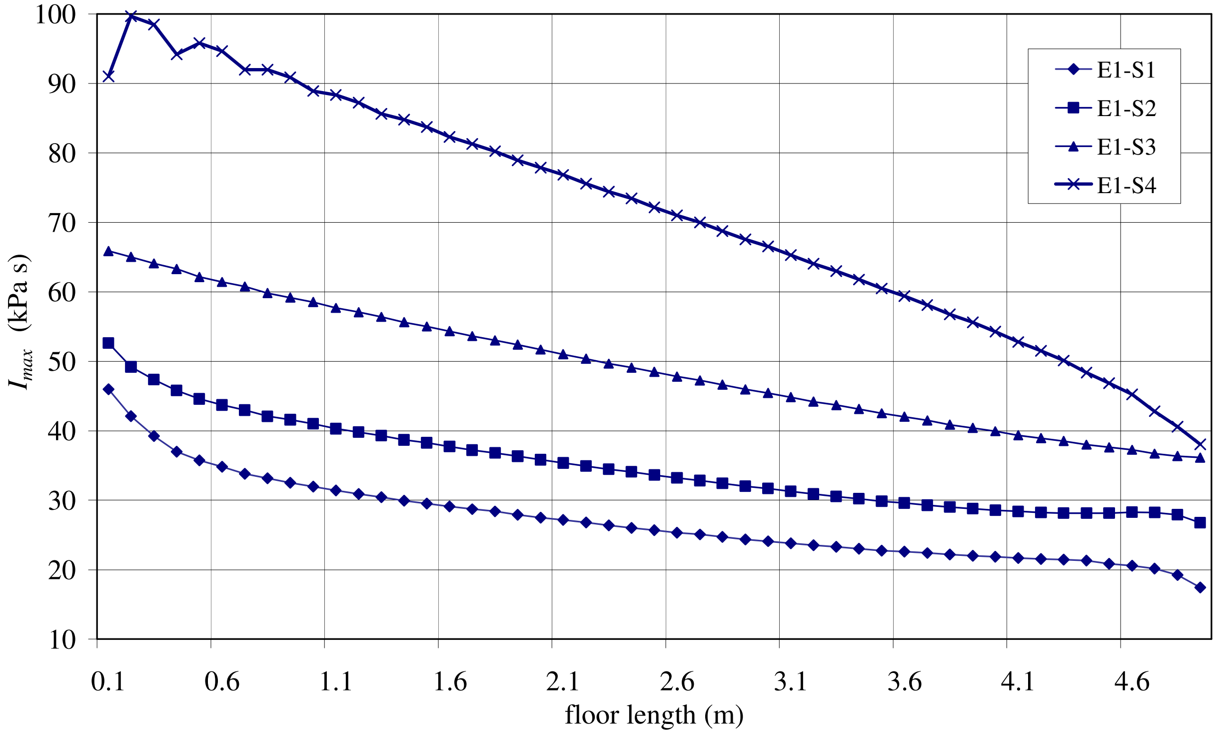

Fig. 8. Maximum impulse along the floor for EOS dry sand and the shear strength varied, E1-S*i*.

The shear strength effect on the maximum impulse is reduced when the EOS is becoming stiffer. However in opposite to maximum pressure it still influences the level of maximum impulse even when the EOS is that of fully saturated clay, see Fig. 9. The average increase in maximum impulse is 1.5 times when E4-S4 is compared with E4-S1.

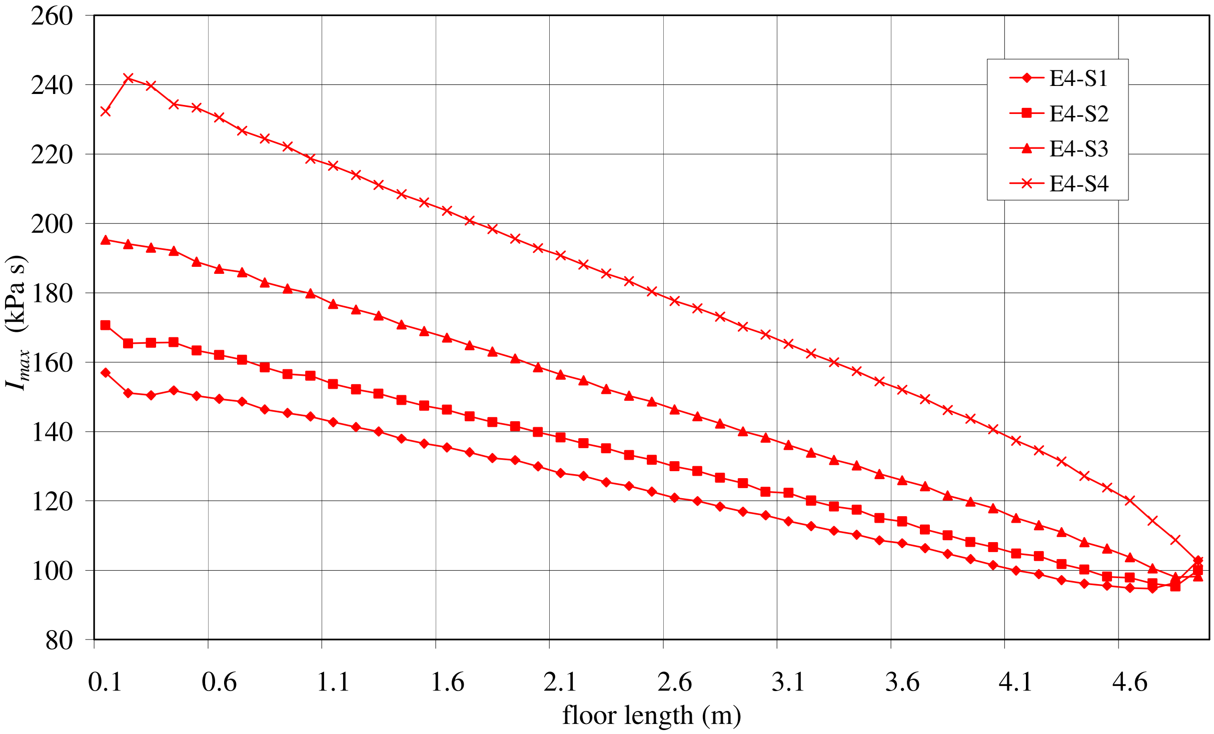

Fig. 9. Maximum impulse along the floor for EOS fully saturated clay and the shear strength varied, E4-S*i*.

The diffraction around the corner was highly influenced by the shear strength. When the shear strength was reduced curl effects started to show up on the floor side. In Fig. 10 and Fig. 11 vector plot field is compared for when the EOS dry sand is kept constant and the strength is varied from dry sand to fully saturated clay, i.e. E1-S1 and E1-S4 respectively. We can first of all see how significant the curl effect is in Fig. 11 compared with Fig. 10. Another interesting detail is that the soil is actually moving upwards from the corner along the wall when we have high shear strength and the soil moving along the floor is almost moving parallel to the floor, see Fig. 10. The moving direction along the wall is totally the opposite when the shear strength is reduced and the soil is actually moving downwards along the wall towards the corner and joining up with the flow under the floor, see Fig. 11. This effect is only occurring in the lower part of the wall. A bit higher up the on the wall the soil starts to move upwards again. Then when the shear strength is low a significant curl effects is occurring just behind the corner on the floor side, which makes the flow of soil not moving parallel along the beginning of the floor.

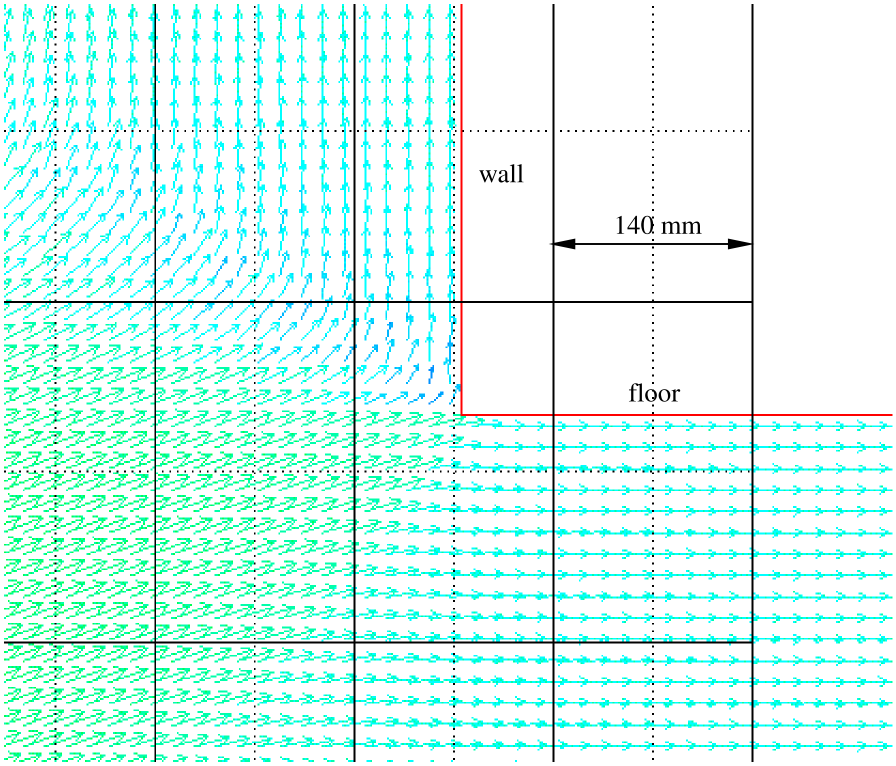

Fig. 10. Vector field plot for EOS dry sand and strength dry sand E1-S1 at 25 ms after detonation. Red arrow = 10 m/s and dark blue arrow = 0 m/s.

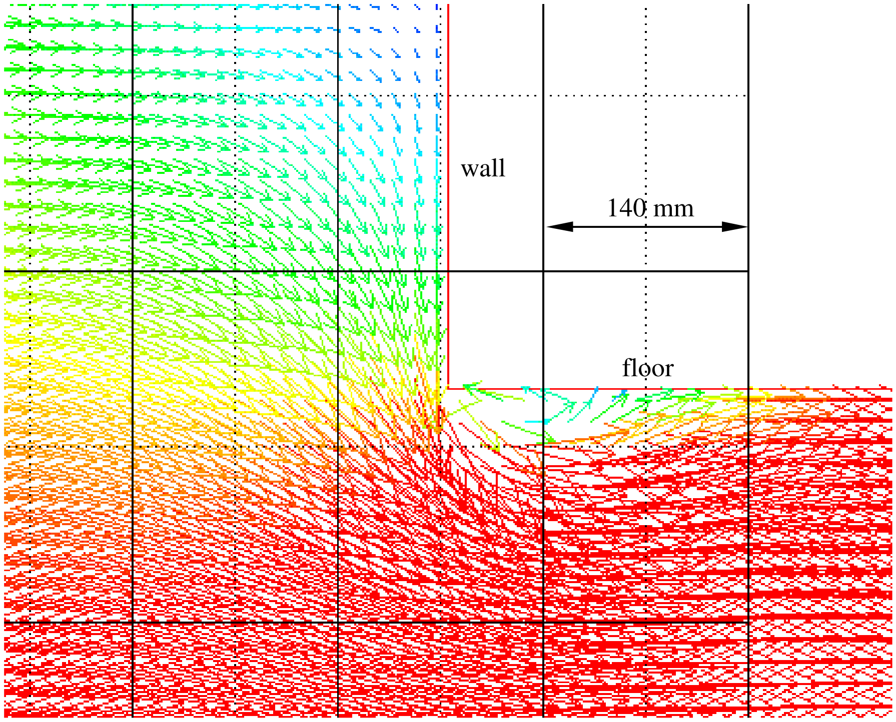

Fig. 11. Vector field plot for EOS dry sand and strength fully saturated clay E1-S4 at 25 ms after detonation. Red arrow = 10 m/s and dark blue arrow = 0 m/s.

## CONCLUSIONS

The influence of the soil properties during shock wave propagation around a rigid block was studied. The results from the simulations clearly show the importance of the soil's EOS. When the EOS is becoming stiffer, i.e. less compressible, it highly influences the maximum pressure and maximum impulse. The shear strength of the soil also affects the maximum pressure and impulse however in lower degree than the EOS.

The maximum pressure along the studied floor of the rigid block was in average increased 132 times when the shear strength was kept constant with dry sands and the EOS was varied from dry sand to fully saturated clay. The maximum pressure along the floor was in average increased three times when the EOS was kept constant with dry sands and the shear strength was varied from dry sand to fully saturated clay. The influence of the shear strength on maximum pressure was highly reduced when the EOS is becoming stiffer. In fact when EOS was kept constant for fully saturated clays and the shear strength was varied from dry sand to fully saturated clay no difference could be seen on maximum pressure.

The maximum impulse along the studied floor of the rigid block was in average increased seven times when the shear strength was kept constant with dry sands and the EOS was varied from dry sand to fully saturated clay. The maximum impulse along the floor was in average increased three times when the EOS was kept constant with dry sands and the shear strength was varied from dry sand to fully saturated clay. The effect of shear strength was reduced when the EOS become stiffer but in opposite of maximum pressure it still was 1.5 times higher when EOS was kept constant for fully saturated clays and the shear strength was varied from dry sand to fully saturated clay.

The diffraction of the ground shock around the corner of the block was small when the soil has high shear strength, the wave did not bend and the wave flowed parallel to the floor with no curl effects. The soil that hit the vertical wall moved upwards when the shear strength was high. The diffraction increased and became significant when the shear strength was set to low. A significant curl effect was detected close to the corner on the floor side. Another interesting result was that the soil flowed down the vertical wall when the shear strength was set to low and joined up with the flow around the floor.

## ACKNOWLEDGEMENTS

The author acknowledges the support given by Swedish Rescue Services Agency and especially Björn Ekengren. Additionally members of the West Sweden Shock Wave Group and especially Dr. Morgan Johansson and Dr. Joosef Leppänen are highly acknowledged for their input. Special thanks to my colleague Ola Pramm Larsen at ANKER - ZEMER Engineering A/S, who performed the large number of simulations, analyzed the results, and prepared them for presentation.

## REFERENCES

[1] Ekengren B. 2006, *Skyddsrum, SR 06*, Swedish Rescue Services Agency, B54-141/06, Karlstad, Sweden.
[2] Century Dynamics Inc., 2004, *AUTODYN Theory Manual Revision 5.0*, San Ramon, CA, USA.
[3] Laine L. and Sandvik A., "Derivation of mechanical properties for sand", *4th Asian-Pacific conference on Shock and Impact Loads on Structures*, CI-Premier PTE LTD, 2001, vol. 4, pp 353-360, Singapore.
[4] Moxnes J. F., Ødegårdstuen G., Atwood A., and Curran P., "Mechanical properties of a porous material studied in a high speed piston driven compaction experiment", 1999, *30th International Annual Conference of ICT Energetic Materials, Fraunhofer Institut Chemische Technologie.*
[5] Heyerdahl H. and Madshus C., 2000, "EOS-data for sand, Tri-axial tests on sand from Sjöbo", Norges Geotekniske institutt, NGI rept. 20001157-1, Oslo, Norway.